



The influence of variable viscosity on delayed cooling due to variable thermal conductivity

A.P. van den Berg^{a,*}, D.A. Yuen^b, E.S.G. Rainey^c

^a *Department of Theoretical Geophysics, Institute of Earth Sciences, Utrecht University, P.O. Box 80.021, Budapestlaan, 3508 TA Utrecht, The Netherlands*

^b *Department of Geology and Geophysics and Minnesota Supercomputer Institute, University of Minnesota, Minneapolis, MN 55455-0219, USA*

^c *Planetary Sciences Division, Code-150-21, Caltech, Pasadena, CA 91125, USA*

Received 29 May 2003; received in revised form 7 January 2004; accepted 7 January 2004

Abstract

Recently it was found for constant viscosity models that variable thermal conductivity can delay significantly the secular cooling of the mantle. We have verified that this same effect also holds up well for variable viscosity, in which we have used up to a factor of 3000 in the lateral viscosity variations due to temperature and a factor of 100 increase from pressure effects. A purely pressure-dependent thermal conductivity does not exert any effect on retarding the secular cooling. The amount of time for the delay is decreased a little by the presence of variable viscosity, but its influence on retarded cooling still remains. We have also found that the cooling predicted by parameterized convection is faster than for the corresponding two-dimensional (2D) solution taken from solving the complete convection equations.

© 2004 Elsevier B.V. All rights reserved.

Keywords: Delayed secular cooling; Variable thermal conductivity; Variable viscosity

1. Introduction

The problem of secular cooling in the mantle has been attracting much attention (Sharpe and Peltier, 1978; Schubert et al., 1979; Davies, 1980; Stevenson et al., 1983) because of the popularity gained by the introduction of parameterized convection using temperature-dependent rheology (McKenzie and Weiss, 1975). The thermal evolution of the mantle is influenced by many physical mechanisms, such

as temperature-dependent viscosity (Tozer, 1972; Sharpe and Peltier, 1978), the nature of convection with nonlinear rheology in the upper mantle (Christensen, 1985; Kawada and Honda, 1999) and depth-dependent viscosity (Hansen et al., 1993; Zhang and Yuen, 1996; Bunge et al., 1996). Aside from few works on the effects of thermal conductivity in mantle convection (Balachandar et al., 1992; Matyska et al., 1994; Tackley, 1996), there has been an hiatus in this important area until the introduction of the semi-empirical thermal conductivity model (Hofmeister, 1999). This model based on solid-state physics can account for both the lattice and radiative heat-transfer mechanisms of mantle materials and can describe the temperature and pressure-dependence of

* Corresponding author.

E-mail addresses: berg@geo.uu.nl (A.P. van den Berg), davey@msi.umn.edu, emma@msi.umn.edu (D.A. Yuen), emma@gps.caltech.edu (E.S.G. Rainey).

the thermal conductivity for a wide suite of mantle materials (Hofmeister, 1999, 2001). This work by Hofmeister has stimulated some recent modelling efforts in unveiling various facets where variable thermal conductivity does make a difference in mantle convection. These interesting effects from variable thermal conductivity include effects on enlarging the hot upwellings in the lower mantle and stabilizing the plumes (Dubuffet and Yuen, 2000; Dubuffet et al., 1999), producing thinner downwellings than for constant thermal conductivity (Dubuffet et al., 2000), Nusselt number versus Rayleigh number scaling relationship in heat transfer (van den Berg et al., 2001), stabilizing of deep mantle plumes by the radiative component of thermal conductivity (Dubuffet et al., 2002), and secular cooling of the mantle (van den Berg et al., 2002; van den Berg and Yuen, 2002). The significant effect of delayed secular cooling by a billion years, which has important ramifications on the Earth's heat budget, was found in the studies by van den Berg and his colleagues. However, all of the above works have been based on constant mantle viscosity and no account, up to now, has been taken on the interaction between variable thermal conductivity and temperature- and pressure dependent viscosity.

In this study we will devote our efforts to the study of the influence of temperature- and pressure-dependent viscosity on variable thermal conductivity convection in the secular cooling problem, since there have been some issues raised concerning the effect of temperature-dependent viscosity in nullifying the delayed cooling effect brought on by variable thermal conductivity. Therefore, our goal in this paper is to determine whether this important result of retarded secular cooling induced by variable thermal conductivity would stand up to the test of variable viscosity. Section 2 will be the model section describing the thermal conductivity model and the numerical techniques. This will be followed by the results section. We will also compare the averaged temperature evolution between fully developed two-dimensional (2D) solutions obtained by solving the coupled partial differential equations and the results arrived at by a single ordinary differential equation within the framework of parameterized convection. In the last section we will discuss the geophysical results and give the conclusions.

2. Model description

Our two-dimensional mantle convection model is based on an extended Boussinesq formulation for an incompressible infinite Prandtl number fluid (Steinbach et al., 1989), defined in the following non-dimensional equations which express conservation of mass, momentum and energy:

$$\partial_j u_j = 0 \quad (1)$$

$$\partial_i \Delta P + \partial_j \tau_{ij} = \alpha Ra T \delta_{i3} \quad (2)$$

$$\frac{DT}{Dt} = \partial_j \kappa \partial_j T + \alpha Di w (T + T_0) + \frac{Di}{Ra} \Phi + RH(t) \quad (3)$$

Here D/Dt in (3) refers to the Lagrangian (substantive) time derivative and the terms scaled with the dissipation number Di describe the non-Boussinesq effects of adiabatic heating and viscous dissipation, respectively. Symbols used in (1)–(3) are defined in Table 1. Quantities have been non-dimensionalized using the following scale parameters: the depth of the convecting layer h as the spatial scale and the thermal diffusion time of the layer $t_0 = h^2/\kappa_0$ for the time scale. The diffusivity scale is expressed as $\kappa_0 = k_0/\rho c_p$, where k_0 is the scale value of the variable conductivity and ρ , c_p are the density and specific heat at constant pressure, respectively, which are constants in our model. Thermal diffusivity $\kappa = k(T, P)/(\rho c_p)$ is based on the temperature and pressure dependent conductivity model of Hofmeister (1999):

$$\begin{aligned} k(T, P) &= k_0 \left(\frac{298}{T} \right)^a \exp \left[- \left(4\gamma + \frac{1}{3} \right) \alpha(P)(T - 298) \right] \\ &\times \left(1 + \frac{K'_0 P}{K_0} \right) + \sum_{i=0}^3 f b_i T^i \end{aligned} \quad (4)$$

The first term in (4) represents a contribution from phonon transport k_{lat} while the second term k_{rad} corresponds to radiative heat transport, where the polynomial coefficients b_i are parameters obtained from fitting spectral data. $k_0 = 4.7 \text{ W m}^{-1} \text{ K}^{-1}$ and the fitting parameter $a = 0.3$ is representative for olivine. In this composite conductivity model both components have opposite temperature dependence, especially in

Table 1
Physical parameters

Symbol	Definition	Value	Unit
h	Height of the domain	3×10^6	m
z	Depth coordinate aligned with gravity	–	–
P	Static pressure	–	–
ΔP	Dynamic pressure	–	–
T	Temperature	–	–
ΔT	Temperature scale value	3500	K
u_i	Velocity field component	–	–
$e_{ij} = \partial_j u_i + \partial_i u_j$	Strain rate tensor	–	–
$e = [1/2 e_{ij} e_{ij}]^{1/2}$	Second invariant of strain rate	–	–
w	Vertical velocity aligned with gravity	–	–
$\eta(T, z) = \eta_0 \exp(cz - bT)$	Temperature and pressure/depth dependent viscosity	–	–
η_0	Viscosity scale value	–	Pa s
$\tau_{ij} = \eta e_{ij}$	Viscous stress tensor	–	–
$\Phi = \eta e^2$	Viscous dissipation function	–	–
$\alpha(z) = \Delta\alpha / ([c(1-z) + 1]^3)$	Depth dependent thermal expansivity	–	–
$\Delta\alpha = \alpha(1)$	–	–	–
$c = \Delta\alpha^{1/3} - 1$	–	–	–
α_0	Thermal expansivity scale value	2×10^{-5}	K^{-1}
ρ	Density	–	–
ρ_0	Density scale value	4000	kg m^{-3}
c_P	Specific heat	1250	$\text{J K}^{-1} \text{kg}^{-1}$
k	Thermal conductivity	–	–
k_0	Conductivity scale value	4.7	$\text{W m}^{-1} \text{K}^{-1}$
a	Conductivity power-law index	0.3	–
γ	Grueneisen parameter	1.2	–
K_0	Bulk modulus	261	GPa
K'_0	Pressure derivative of bulk modulus	5	–
b_0	Coefficient phonon conductivity	1.7530×10^{-2}	–
b_1	–	-1.0365×10^{-4}	–
b_2	–	2.2451×10^{-7}	–
b_3	–	-3.4071×10^{-11}	–
$\kappa = k(T, P) / (\rho c_P)$	Thermal diffusivity	–	–
g	Gravitational acceleration	9.8	m s^{-2}
$H(t) = H_0 \exp(-t/\tau)$	Time-dependent internal heating	–	W kg^{-1}
τ	Dimensional decay time of radioactive heating	3.6	Gyr
H_0	Dimensional value of internal heating	–	W kg^{-1}
$R = H_0 h^2 / c_P \kappa_0 \Delta T$	Non-dimensional internal heating number	–	–
	$R = 20 \leftrightarrow H_0 = 9.2 \times 10^{-12} \text{ W kg}^{-1}$		
$Ra = \rho_0 \alpha_0 g \Delta T h^3 / \kappa_0 \eta_0$	Rayleigh number	$10^6 < Ra < 10^7$	–
$Di = \alpha_0 g h / c_P$	Dissipation number	0.47	–

the derivatives with respect to temperature. Whereas k_{lat} decreases with increasing temperature, k_{rad} is an increasing function of temperature. The parameter f in the radiative part controls the predominance of the two mechanisms. $f = 1$ corresponds to the Hofmeister (1999) model and $f > 1$ has recently been shown to control the occurrence of boundary layer instabilities near a hot core-mantle boundary (Dubuffet et al., 2002).

We use a variable temperature (T) and pressure (P) or depth (z) dependent viscosity model. The delaying effect of temperature dependence of viscosity on secular cooling through the negative feedback on the vigor of convection is well known (Tozer, 1972). On the other hand, we (van den Berg et al., 2002) have shown recently that variable conductivity models including temperature dependence are characterized by a shallow low thermal conductivity zone, resulting

in a higher temperature in the top part of the upper mantle (van den Berg et al., 2001). In models with temperature dependent viscosity higher temperatures at shallow depth will cause a more pronounced asthenosphere which facilitates global heat-transport to the surface, resulting in an increased cooling rate compared to a constant viscosity case. Therefore, we will investigate the impact of variable conductivity on the secular cooling evolution of convecting planets and at the same time include the effect of temperature dependent viscosity, because of the multiple nonlinear feedback mechanisms involved.

The variable viscosity is Newtonian and is parameterized in terms of non-dimensional depth z and temperature T ,

$$\eta(T, z) = \eta_0 \exp(cz - bT) \quad (5)$$

where c , b are defined as the natural logarithm of the viscosity contrasts across the convecting layer due to pressure ($\Delta\eta_P$) and temperature ($\Delta\eta_T$), respectively. The viscosity contrast due to pressure $\Delta\eta_P$ is fixed to 100. For the viscosity contrast due to temperature we have used $\Delta\eta_T = 3000$ for most of the results shown and a contrasting value of 300 for comparison. The Rayleigh number, based on the surface physical parameters, is around 10^6 . For further details, the reader should consult Table 1.

The governing equations are solved on a rectangular domain with a layer depth of 3000 km and an aspect ratio of 2.5. Free-slip, impermeable boundaries are used for the Stokes Eq. (2). The model is completely heated from within with a zero heat flux bottom boundary in order to focus just on the secular cooling behavior of the convecting mantle. The top boundary is kept at 273 K and zero heatflux conditions are applied to the vertical boundaries. The internal heating is parameterized by a uniform distribution with exponential decay given by a half-life time of 2.5 Gyr. The transient convection experiments are started from an initial temperature distribution obtained from a statistically steady-state model with stronger constant heating characterized by an internal heating number $R = 40$ (Leitch and Yuen, 1989) with a CMB temperature of about 3773 K. The equations are solved using finite element methods using the SEPRAN finite element package, (<http://dutita0.twi.tudelft.nl/sepran/sepran.html>). We use 10^4 quadratic elements for the Stokes Eq. (2) and

four times as many linear elements for the energy equation (van den Berg et al., 1993), resulting in a grid resolution of 150 points and 140 points in the horizontal and vertical directions, respectively. More points are needed for variable conductivity calculations than constant conductivity (van den Berg et al., 2001). Gridpoint spacing is uniform in the horizontal direction and grid refinement is applied near the horizontal boundary layers, with point spacing of 6 km, to resolve strong gradients of both the viscosity and conductivity, in particular at shallow depth. The Stokes equation is solved using a penalty method with the penalty parameter $\epsilon = 10^{-6}$. The discrete coupled system of finite element equations is driven by the time dependent energy equation which is integrated in time using a predictor corrector method (van den Berg et al., 1993).

3. Results

First we show the temporal evolution of a model with variable conductivity and temperature and pressure-dependent viscosity. Fig. 1 shows two snapshots of the temperature, viscosity, streamfunction and the lateral variation of the effective conductivity, at different integration times corresponding to 0.91 and 4.25 Gyr, respectively. The early snapshot (a) is characterized by a hot interior with amplitudes of temperature variations limited to 700 K in the interior of the domain. The pressure and temperature dependent logarithmic viscosity is shown in frames (c and d). The viscosity plots show a background field characterized by a low viscosity zone in the upper part of the domain which is broader in the high T snapshot. Correlation with the temperature field can be clearly seen in the cold downwellings and in the general increase of the viscosity resulting from the secular cooling. The flow field is dominated by fast cold downwellings at the vertical boundaries, and more diffuse upwelling away from the vertical boundaries with some concentration in the upper mantle, as illustrated by the streamfunction field shown in (c). The second snapshot (b), after another 3 Gyr of secular cooling, is dominated by slab-like cold downwellings in the interior domain, showing penetration of the cold slab-like features into the high viscosity (Fig. 1d) hotter lower mantle. The corresponding streamfunction frame (Fig. 1f) again shows concentration of the flow in the upper mantle.

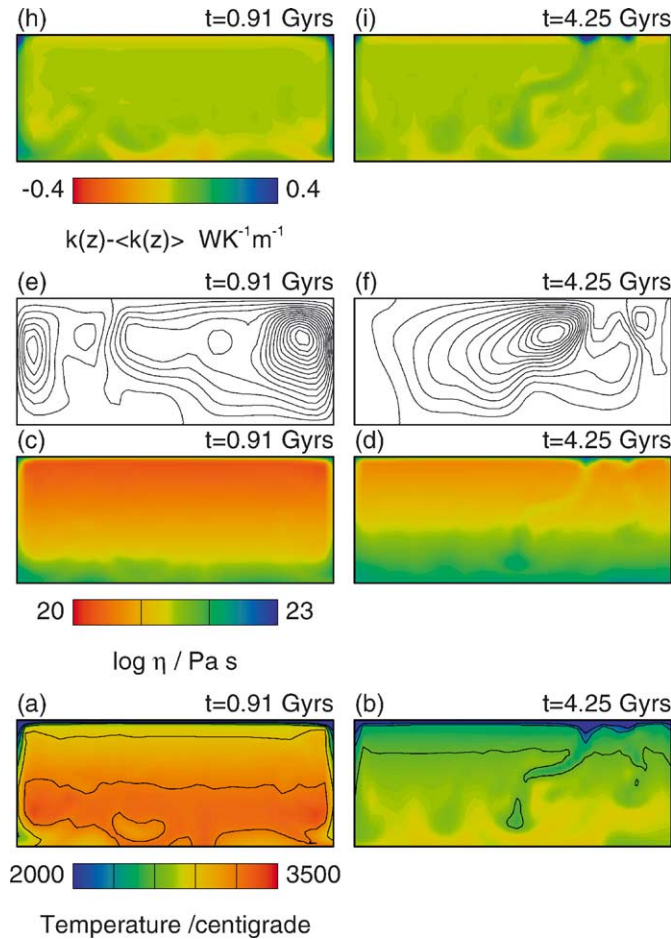


Fig. 1. Temperature (a and b); viscosity (c and d); streamfunction (e and f); and lateral variation of the thermal conductivity (h and i); for two integration times $t = 0.9 \times 10^9$ yr and $t = 4.2 \times 10^9$ yr, to illustrate the effect of secular cooling. Results are for a model with variable $k(P, T)$ and the surface Rayleigh number $Ra = 8 \times 10^5$. The initial value of the time dependent temperature at the core-mantle boundary T_{CMB} is approximately 3800 K. The finite element grid consists of 150 evenly spaced points horizontal and 140 points in the vertical direction with grid refinement near the top and bottom boundary.

Fig. 1h and i shows the lateral variation δk of the corresponding temperature and pressure dependent conductivity fields. The plots illustrate the strong spatial correlation between δk and the temperature field where the variation of the conductivity with pressure has been removed in the subtraction of the horizontal average. The weak low conductivity region at the top of the mantle in Fig. 1e and f mainly results from the removal of the lateral average which is dominated by the strong positive conductivity anomalies at shallow levels in the cold downwellings. This may have implications for the issue regarding thermal assimilation

of the subducting slab (van der Hilst and Karason, 1999).

The background conductivity field also shows a much broader low conductivity zone (LCZ) (van den Berg and Yuen, 2002) which results from the contrasting pressure and temperature sensitivity of the conductivity with $\partial k / \partial T < 0$, $\partial k / \partial P > 0$. This 1D LCZ has been filtered out in the computation of the lateral variation. Profiles of the total conductivity field including the LCZ are shown in Fig. 2.

Vertical profiles of the top 300 km of the upper mantle are shown in Fig. 2 for horizontally averaged

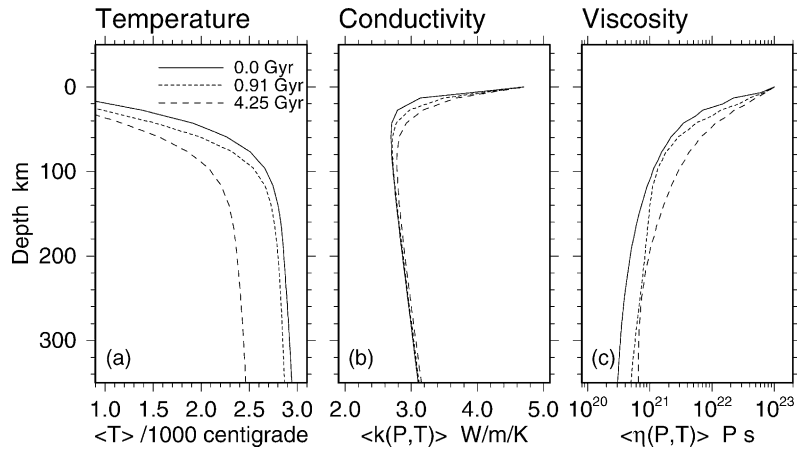


Fig. 2. Vertical profiles of horizontally averaged values of temperature (a); thermal conductivity (b); and viscosity (c); for the same variable conductivity model and integration times (plus initial time) of Fig. 1. Only the upper 10%, 300 km of the model are shown to bring out the sharp variations in the top boundary layer.

temperature, conductivity and viscosity at different model integration times. The geotherms of Fig. 2a show a total cooling of about 500 K over the 4.25 Gyr time window. Fig. 2b shows the sharp boundary layer

characteristics of the T, P dependent variable conductivity, with a shallow low conductivity zone and a strong conductivity variation near the cold boundary similar but much sharper as compared to the vis-

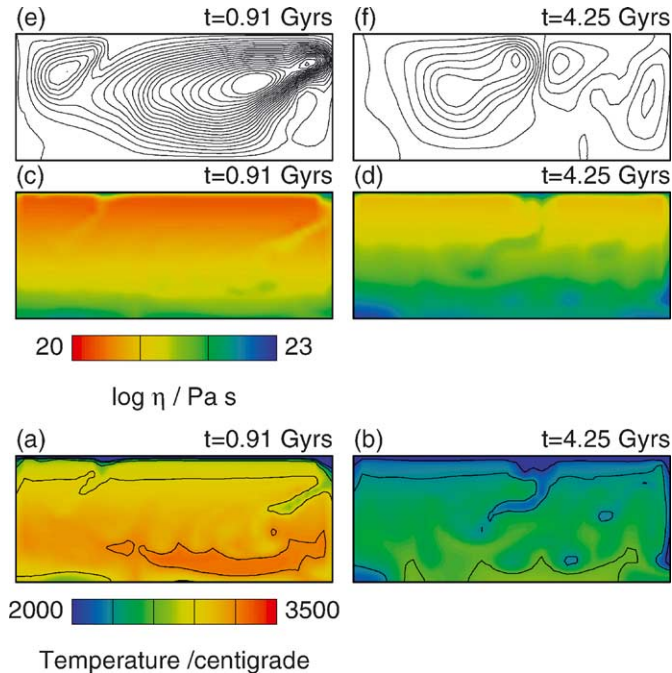


Fig. 3. Temperature (a and b); viscosity (c and d); and streamfunction (e and f); for the same integration times $t = 0.9 \times 10^9$ yr and $t = 4.2 \times 10^9$ yr as in Fig. 1. Results are for a model with constant conductivity $k_0 = 4.7 \text{ Wm}^{-1} \text{ K}^{-1}$ and for the same Rayleigh number $Ra = 8 \times 10^5$ and initial value of T_{CMB} , approximately 3800 K as in Fig. 1.

cosity distribution shown in Fig. 2c. The different snapshots shown illustrate the increase of both the conductivity and the viscosity fields during secular cooling.

Next we turn to the case with constant thermal conductivity. We have used the same effective Rayleigh number for both the constant and variable conductivity cases, in order to make the comparison. This type of comparison between variable and constant thermal conductivity models has been described in van den Berg et al. (2002). Fig. 3 shows the snapshots of temperature, the logarithmic viscosity and streamfunction for a model with the same parameters as shown in Fig. 1 apart from the conductivity model which is constant here, for the same time instants as in Fig. 1. We emphasize here the principal difference between Figs. 1 and 3 is the increased degree of cooling apparent from frames Fig. 3b and corresponding higher viscosity Fig. 3d.

In Fig. 4 we show the time series of volumetrically averaged temperature (Fig. 4a and b) and viscosity (Fig. 4c and d), over a logarithmic time-scale. A com-

parison is made between variable conductivity models plotted as solid curves and constant conductivity models shown as dotted lines. Two model classes are considered, which are different by an order of magnitude in the temperature dependence of the viscosity, characterized by the thermal viscosity contrast across the layer depth, shown in the left and right hand column, respectively. The temperature curves in Fig. 4a and b show clearly a delay in the secular cooling from 1 to 2 Gyr, for the variable conductivity models compared to the corresponding constant conductivity cases. A similar delay effect due to variable conductivity was already observed for isoviscous models in (van den Berg et al., 2002; van den Berg and Yuen, 2002). The results shown here illustrate that this delay also is a robust phenomenon in models with variable temperature and pressure dependent viscosity. The differences in the cooling rate and internal temperature are reflected in the curves for the volumetrically averaged effective viscosity, resulting in consistently lower viscosity, up to a factor of two, for the slower cooling variable conductivity models. Fig. 5 shows similar results as given

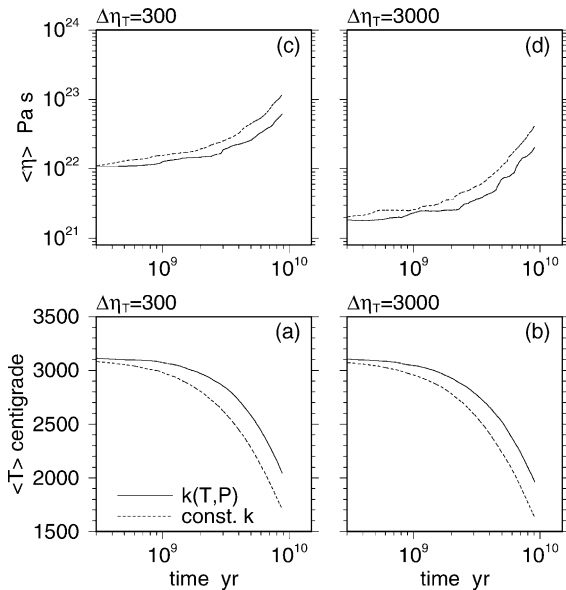


Fig. 4. Time series results for a model with variable conductivity $k(T, P)$ (solid lines), compared to a model with constant conductivity k_0 (dashed lines). Volume averaged temperature (a and b); and viscosity (c and d); are shown for two values of the thermal viscosity contrast $\Delta\eta_T = 300$ (a and c); and 3000 (b and d). The surface Rayleigh number $Ra = 8 \times 10^5$, and the viscosity contrast due to pressure $\Delta\eta_P = 100$.

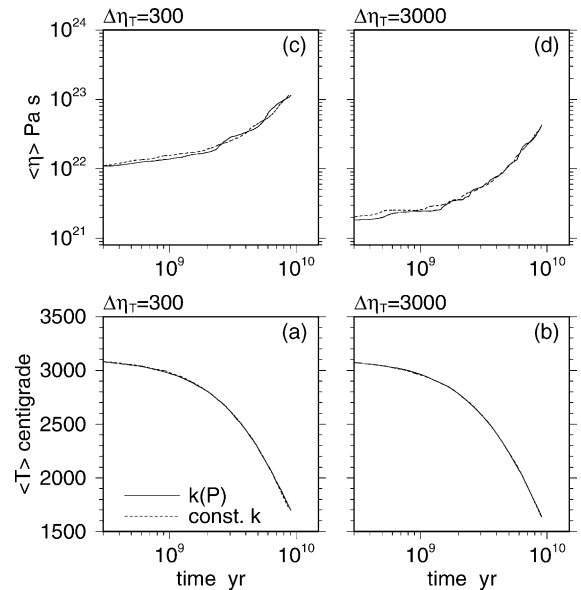


Fig. 5. Time series as in Fig. 4 but with purely depth dependent conductivity $k(P)$ (solid lines), compared to a model with constant conductivity k_0 (dashed lines). Volume averaged temperature (a and b); and viscosity (c and d); are shown for two values of the thermal viscosity contrast $\Delta\eta_T = 300$ (a and c); and 3000 (b and d). The surface Rayleigh number $Ra = 8 \times 10^5$, and the viscosity contrast due to pressure $\Delta\eta_P = 100$.

in Fig. 4 for corresponding models with a purely depth dependent conductivity model, obtained by substitution of the surface value for the temperature in the conductivity expression (Eq. (4)). The results show a negligible difference in the secular cooling behavior and the corresponding viscosity evolution. This result clearly illustrates the key role played by the temperature dependence of the conductivity in reducing the efficiency of convective heat transport and the overall cooling rate, since pressure dependence alone does not exert any visible effect. We can basically explain this behavior by the faster thermal decay of cold downwellings due to the increased background temperature of the shallow mantle in models with temperature dependent conductivity (van den Berg et al., 2002), as compared to the fully depth dependent case. The decaying thermal buoyancy mainly drives thermal con-

vection in a ‘cooling from the top’ set up with adiabatic bottom boundary and fixed temperature top surface, as applied in our models. Comparing Figs. 4 and 5 the results underscore strongly the inadequacy of applying a purely depth dependent conductivity or a constant viscosity model (DeLandro-Clarke and Jarvis, 1997) in modelling accurately long term cooling behavior.

The impact on secular cooling of the variable conductivity model and the depth dependent conductivity model of Figs. 4 and 5 is further illustrated in Fig. 6 in a number of corresponding temperature snapshots for integration times covering a large portion of the planetary history. The time labeled in million years is increasing from the top down. A prominent characteristic of these results is the slower cooling of the variable conductivity model shown in the left hand column. The results for the depth dependent model

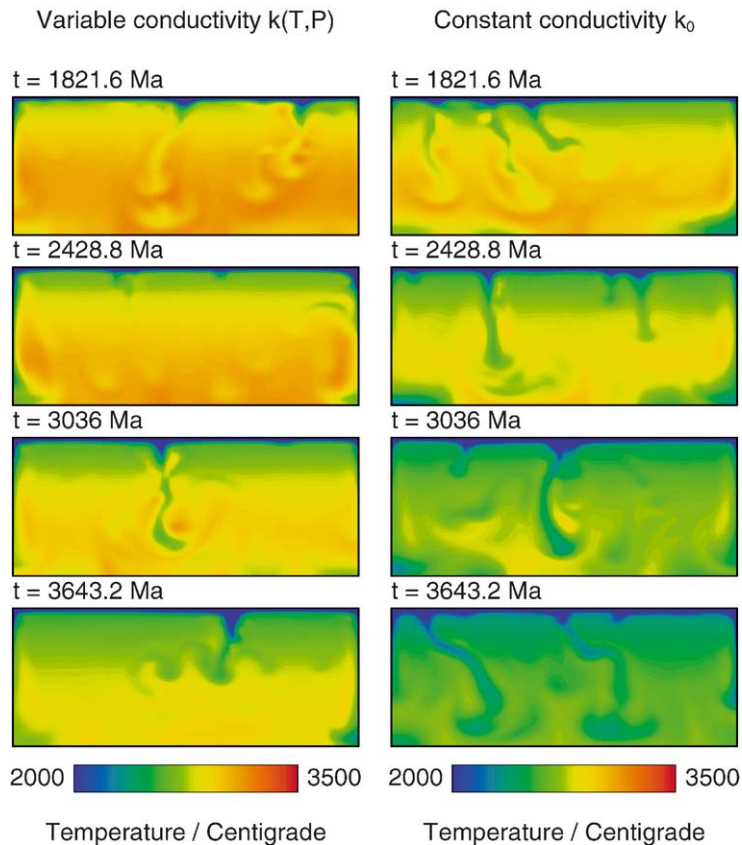


Fig. 6. Comparison of corresponding temperature snapshots between model cases with variable conductivity (as in Fig. 1) (left hand column) and constant conductivity (as in Fig. 2) (right hand). The temperature scale has been reduced to emphasize the cold downwellings. Integration time, increasing in the top down direction, is used in the individual frame labels.

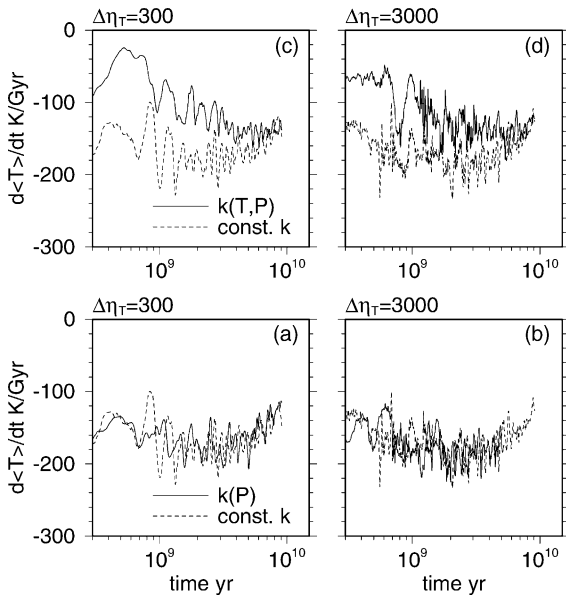


Fig. 7. Cooling rates $d\langle T \rangle / dt$ as a function of time for different temperature dependence of the viscosity $\Delta\eta_T = 300$ (a and c); and $\Delta\eta_T = 3000$ (b and d); for two different conductivity models: the depth dependent conductivity model $k(P)$ (a and b) and as in Fig. 5 and the variable $k(T, P)$ model (c and d) as in Fig. 4.

show a consistently more pronounced cold downwellings. The longevity of cold temperature anomalies which drive the convective flow is directly influenced by the particular thermal conductivity model used.

Fig. 7 shows the time series of the secular cooling rate for several conductivity models and for the same two viscosity models as in Fig. 4. The cooling rate has been computed by central time differencing the time series of the volume averaged mantle temperature followed by a seven point symmetric boxcar moving average filter operation to remove the round-off noise signal. The curves in the right hand column show faster fluctuations in time and higher values of the cooling rate, inline with the lower viscosity values for these cases with stronger temperature dependence of the viscosity. As in Figs. 5 and 6 results are compared between the depth dependent conductivity model $k(P)$ Fig. 7a and b and the variable conductivity model $k(T, P)$ Fig. 7c and d. Both these cases are compared with the constant conductivity case k_0 (dashed curves). The constant conductivity results show a cooling rate roughly in the range 150,200 K per billion years with decreasing values at times close to the age of the Earth.

Again, the depth-dependent conductivity models in Fig. 7a and b show similar values as the constant conductivity models, very much in line with the closeness of the temperature results shown in Fig. 5. This situation is different for the variable conductivity models in Fig. 7c and d, showing reduced cooling rates by some 100 K per billion years early in the history and decreasing difference with increasing model time. We also note the opposite trend in the variable conductivity cases with cooling rate increasing with time compared to the constant conductivity case which shows weakly decreasing cooling rate with increasing time. This effect reflects the negative feedback between temperature and conductivity and its impact on both conductive cooling through the cold and highly viscous top boundary layer and convective cooling driven by the more rapid diffused cold downwellings (Dubuffet et al., 2000).

The effect of the initial temperature distribution on the differences in secular cooling between different models is shown in Fig. 8 where the delay in secular cooling due to variable conductivity is compared between models with different initial temperature expressed by the approximate temperature of the adiabatic boundary at the core-mantle boundary. Fig. 8 shows that the cooling delay in variable conductivity persists for hotter initial temperature distributions.

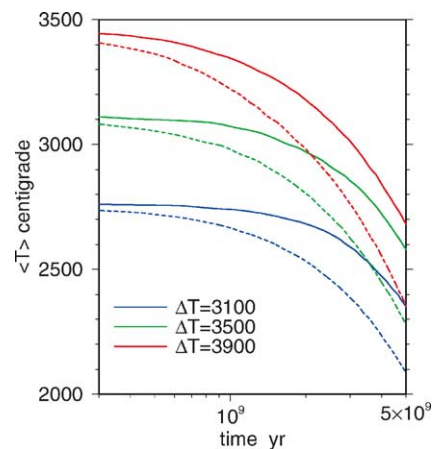


Fig. 8. Delay in secular cooling for variable conductivity models with different initial temperature contrast across the mantle ΔT . The slower cooling top curve of each pair corresponds to the variable conductivity case, the faster cooling one is for the corresponding constant conductivity model.

At model times around 4 Gyr differences in cooling amount about 200–300 K, increasing with the initial temperature. This shows that the results are robust within the range of uncertainty of the initial temperature at the CMB.

In Fig. 9 we compare the results for different Rayleigh numbers. Time series are shown for the surface heatflux (bottom), volume averaged temperature (middle) and volume averaged viscosity (top), using solid lines for variable conductivity models and dashed lines for constant conductivity cases. The high Rayleigh number models shown in the left hand column cool faster, as shown by the higher surface heatflux and faster decrease of the volume averaged temperature. The cooling delay between variable and

constant conductivity models is slightly greater for the high Ra cases.

Fig. 10 shows the same volume averaged temperature curves as displayed in Fig. 9c and d together with corresponding cooling curves obtained from a parameterized convection model (e.g. Schubert et al., 1979) for the volume averaged convection model based on a powerlaw relation between Nusselt and Rayleigh number with powerlaw exponent $\beta = 1/3$, given by

$$\frac{d}{dt} \langle T(t) \rangle = \frac{H(0)}{C} \exp\left(\frac{-t}{\tau}\right) - \frac{\langle k(t) \rangle}{Ch^2} (\langle T(t) \rangle - T_s)^{1+\beta} \times \left[\frac{\rho \alpha g h^3 C}{\langle k(t) \rangle \langle \eta(t) \rangle Ra_C} \right]^\beta \quad (6)$$

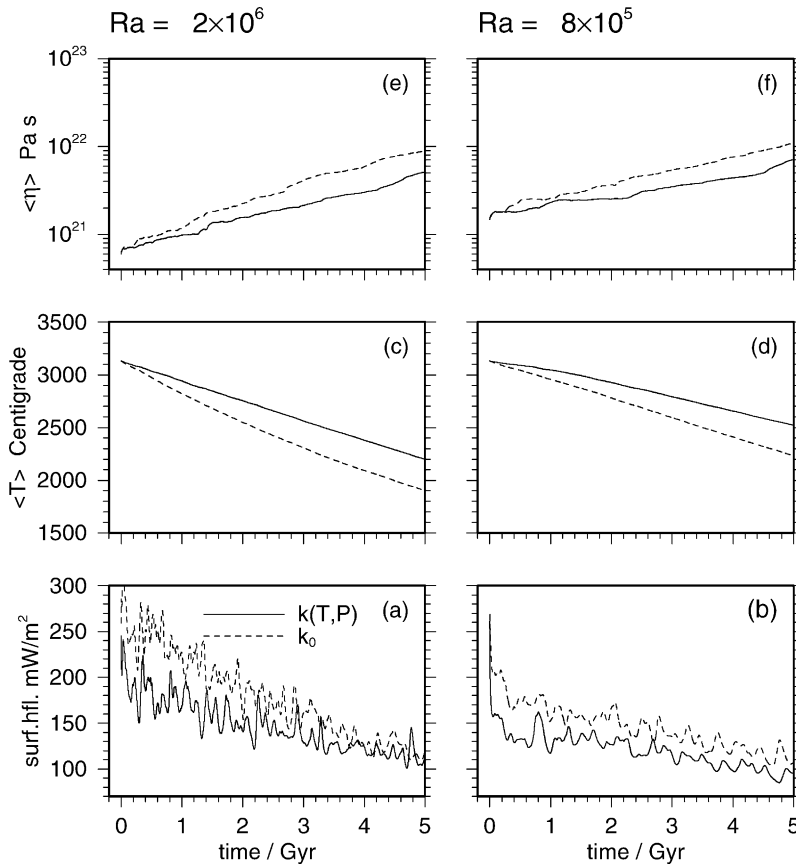


Fig. 9. Influence of the surface Rayleigh number on the delay in secular cooling due to variable conductivity illustrated in time series of surface heatflux (a and b); volume averaged temperature (T) (c and d); and volume averaged viscosity (e and f). The left hand column (a, c and e) with higher Rayleigh number $Ra = 2 \times 10^6$ shows faster cooling compared to the lower Ra case (b, d and f) with $Ra = 8 \times 10^5$. The delay in secular cooling is slightly greater for the higher Ra case.

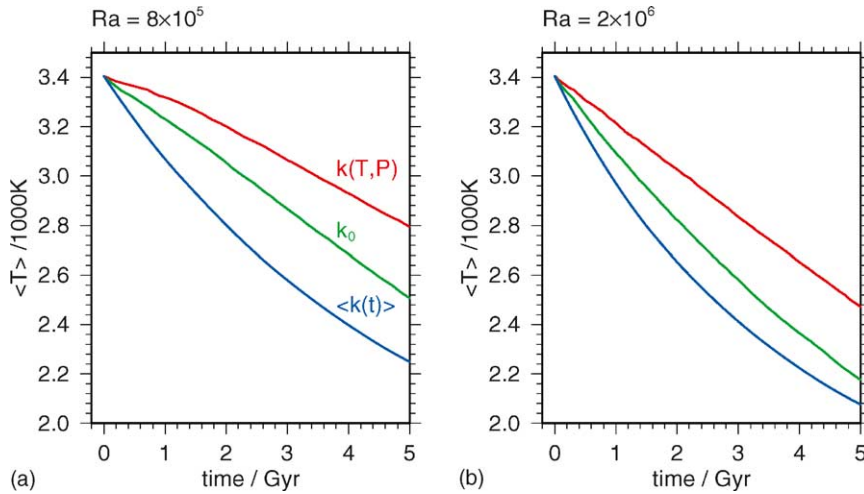


Fig. 10. Volume averaged temperature as a function of time for two values of the Rayleigh number. Comparison of 2D full convection model results for variable conductivity (red curves labeled $k(T, P)$) and constant conductivity (green curves labeled k_0). The blue curves labeled $\langle k(t) \rangle$ represent corresponding results of a parameterized convection model based for the volume average temperature using time series of volume averaged conductivity $\langle k(t) \rangle$ and viscosity $\langle \eta(t) \rangle$ taken from the full convection model (blue curves labeled $\langle k(t) \rangle$).

In the ODE (6) time dependent values of the volume average values for the conductivity $\langle k(t) \rangle$ and viscosity $\langle \eta(t) \rangle$ were substituted, obtained from postprocessing the fully 2D convection results. For both Rayleigh number cases shown here, the parameterized convection model predicts a much too fast secular cooling,

even faster than the constant conductivity case. Clearly the parameterized convection results are off by up to 500 K in temperature and faster by more than 2 Gyr in time than for variable thermal conductivity results.

Fig. 11 shows the results of the parameterized convection model using different parameterizations for

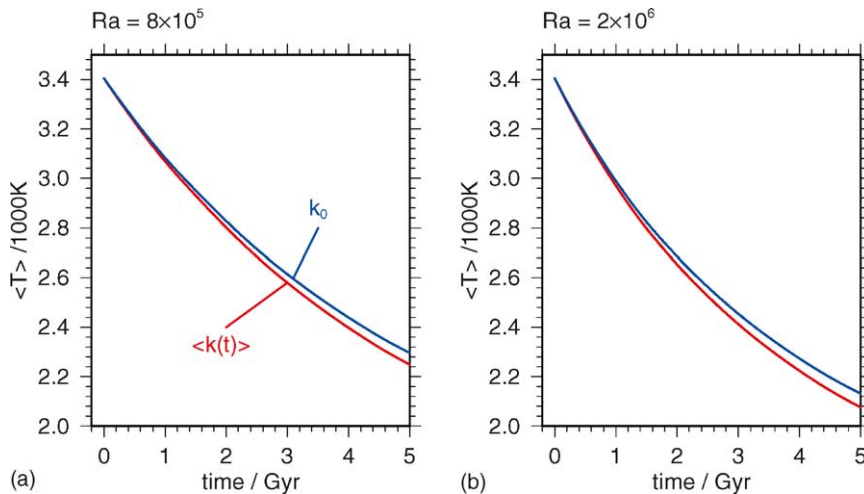


Fig. 11. Comparison of parameterized convection results for different conductivity parameterizations. Red curves labeled $\langle k(t) \rangle$ are for a model using time dependent volume averaged conductivity taken from a corresponding full convection run with variable conductivity $k(T, P)$. Blue curves labeled k_0 are for a model with constant conductivity. Notice the parameterized convection predicts a faster secular cooling for the variable conductivity case, in contrast to the results for full 2D convection.

the conductivity for the same two Rayleigh numbers as in Figs. 9 and 10. The top curve in each frame is for a model using constant conductivity and the bottom curve is based on time dependent volume averaged conductivity values obtained from postprocessing the full convection model results. Both frames show the variable conduction parameterized model to cool faster than the corresponding constant conductivity case. This is in direct contrast to the results obtained from the fully 2D convection results.

4. Concluding remarks

Recently we (van den Berg et al., 2002; van den Berg and Yuen, 2002) have found that the variable thermal conductivity could delay secular cooling for a constant viscosity model by around O(Ga). It is therefore vitally important to confirm these results within an Earth model with variable viscosity. To delineate the nonlinear interaction between variable viscosity and conductivity we have employed a model with a purely depth-dependent thermal conductivity $k(P)$ and variable viscosity and found that the retardation effect with respect to the corresponding uniform conductivity case is definitely absent. This means that variable conductivity, vis a vis $k(T, P)$, provides the necessary nonlinear feedback to the system, whereas $k(P)$ does not exert any feedback at all on the temperature evolutionary equation (Eq. (3)). In this work we have employed a viscosity which depends on both temperature and depth or pressure (Eq. (5)). Variations in the temperature-dependent viscosity were set at 3000, while there was a two-order of magnitude of increase in the viscosity with depth (Mitrovica and Forte, 2002). In all cases we have found that the delayed cooling effect is retained in the presence of variable viscosity. These results are further strengthened by our comparing the 2D solution with the 1D solution obtained from parameterized convection. We found that the parameterized convection model delivers the fastest cooling rate, with the variable thermal conductivity and variable viscosity 2D solutions having the slowest cooling rate. These results make our previous findings much more robust and endow it with greater geophysical relevance. However, there remains a serious shortcoming in this model and this has to do with the adiabatic thermal condition im-

posed at the core–mantle boundary. We must assess this flaw by using a core–coupling model of the genre proposed by Steinbach et al. (1993). We have already begun to study these effects with such a core–coupling model in which the temperature at the core–mantle boundary evolves with time (Rainey et al., 2002).

What then are the implications of delayed secular cooling on mantle thermal evolution? First, the influence of initial conditions (Solomatov, 2001) on thermal evolution might be more important than has been appreciated. Second, as shown in previous work (van den Berg et al., 2002) variable conductivity models are characterized by a higher internal temperature, compared to constant conductivity models, due to the shallow low conductivity zone. As a result the lower mantle today would be hotter with a variable thermal conductivity model than with a constant conductivity model. This would mean that an enriched radiogenic layer in the abyssal portion of the lower mantle (Kellogg et al., 1999) would be more subject to partial melting since the temperatures would lie close to the solidus of lower mantle materials (Boehler, 2000). Within the context of a thermal–chemical convection model with mechanical heating, variable viscosity, and constant thermal conductivity, Hansen and Yuen (2000) have already pointed out to this aspect of deep mantle enriched layers. Thus the variable conductivity model puts further constraints on the amount of internal heating in enriched deep mantle layers.

Acknowledgements

We acknowledge constructive comments by an anonymous reviewer and stimulating discussions on the thermal properties in the lower mantle with Anne M. Hofmeister, Tomo K.B. Yanagawa, Ulli Hansen and Satoru Honda. This research has been supported by both the Dutch NWO and the geophysics program of the National Science Foundation.

References

- Balachandar, S., Yuen, D.A., Reuteler, D., 1992. Time-dependent three-dimensional compressible convection with depth-dependent properties. *Geophys. Res. Lett.* 19, 2247–2250.
- Boehler, R., 2000. High-pressure experiments and the phase diagram of lower mantle and core materials. *Rev. Geophys.* 38 (2), 221–245.

- Bunge, H.-P., Richards, M.A., Baumgardner, J.R., 1996. Effect of depth-dependent viscosity on the planform of mantle convection. *Nature* 379, 436–438.
- Christensen, U.R., 1985. Thermal evolution models for the Earth. *J. Geophys. Res.* 90, 2995–3008.
- Davies, G.F., 1980. Thermal histories of convective Earth models and constraints on radiogenic heat production in the Earth. *J. Geophys. Res.* 85, 2517–2530.
- DeLandro-Clarke, W., Jarvis, G.T., 1997. Numerical models of mantle convection with secular cooling. *Geophys. J. Int.* 129, 183–193.
- Dubuffet, F., Yuen, D.A., Rabinowicz, M., 1999. Effects of a realistic mantle thermal conductivity on the patterns of 3-D convection. *Earth Planet. Sci. Lett.* 171, 401–409.
- Dubuffet, F., Yuen, D.A., 2000. A thick pipe-like heat-transfer mechanism in the mantle: nonlinear coupling between 3-D convection and variable thermal conductivity. *Geophys. Res. Lett.* 27 (1), 17–20.
- Dubuffet, F., Yuen, D.A., Yanagawa, T., 2000. Feedback effects of variable thermal conductivity on the cold downwellings in high Rayleigh number convection. *Geophys. Res. Lett.* 27 (18), 2981–2984.
- Dubuffet, F., Yuen, D.A., Rainey, E., 2002. Controlling thermal chaos in the mantle by positive feedback from radiative thermal conductivity. *Nonlinear Process Geophys.* 9 (3–4), 311–323.
- Hansen, U., Yuen, D.A., Kroening, S.E., Larsen, T.B., 1993. Dynamical consequences of depth-dependent thermal expansivity and viscosity on mantle circulations and thermal structure. *Phys. Earth Planet. Inter.* 77, 205–223.
- Hansen, U., Yuen, D.A., 2000. Extended-Boussinesq thermal-chemical convection with moving heat sources and variable viscosity. *Earth Planet. Sci. Lett.* 176, 401–411.
- Hofmeister, A.M., 1999. Mantle values of thermal conductivity and the geotherm from phonon lifetimes. *Science* 283, 1699–1706.
- Hofmeister, A.M., 2001. Thermal conductivity of spinels and olivines from vibrational spectroscopy at ambient conditions. *Am. Mineral.* 86, 1188–1208.
- Kawada, Y., Honda, S., 1999. Parametrization of heat transport by non-Newtonian convection. *Geophys. J. Int.* 137, 441–448.
- Kellogg, L.H., Hager, B.H., van der Hilst, R.D., 1999. Compositional stratification in the deep mantle. *Science* 283, 1881–1884.
- Leitch, A., Yuen, D.A., 1989. Internal heating and thermal constraints on the mantle. *Geophys. Res. Lett.* 16, 1407–1410.
- Matyska, C., Moser, J., Yuen, D.A., 1994. The potential influence of radiative heat transfer on the formation of megaplumes in the lower mantle. *Earth Planet. Sci. Lett.* 125, 255–266.
- McKenzie, D.P., Weiss, N.O., 1975. Speculations on the thermal and tectonic history of the Earth. *Geophys. J. R. Astr. Soc.* 42, 131–174.
- Mitrovica, J.X., Forte, A.M., 2002. On the radial profile of mantle viscosity. In: Mitrovica, J.X., Vermeersen, B.L.A. (Eds.), *Ice Sheets, Sea Level and the Dynamic Earth*, Geodynamics Series 20. American Geophysical Union, Washington, DC, pp. 187–199.
- Rainey, E.S.G., van den Berg, A.P., Yuen, D.A., 2002. Secular cooling rates of the mantle: various influences. *Eos. Trans. AGU* 83 (47), F16.
- Schubert, G., Cassen, P., Young, R.E., 1979. Subsolidus convective cooling histories of terrestrial planets. *Icarus* 38, 192–211.
- Sharpe, H.N., Peltier, W.R., 1978. Parameterized mantle convection and the Earth's thermal history. *Geophys. Res. Lett.* 5, 737–740.
- Solomatov, V.S., 2001. Grain size-dependent viscosity convection and the thermal evolution of the Earth. *Earth Planet. Sci. Lett.* 191, 203–212.
- Steinbach, V., Hansen, U., Ebel, A., 1989. Compressible convection in the Earth's mantle: a comparison of different approaches. *Geophys. Res. Lett.* 16, 633–635.
- Steinbach, V., Yuen, D.A., Zhao, W., 1993. Instabilities from phase transitions and the timescales of mantle evolution. *Geophys. Res. Lett.* 20, 1119–1122.
- Stevenson, D.J., Spohn, T., Schubert, G., 1983. Magnetism and thermal evolution of the terrestrial planets. *Icarus* 54, 466–489.
- Tackley, P.J., 1996. Effects of strongly variable viscosity on three-dimensional compressible convection in planetary mantles. *J. Geophys. Res.* 101, 3311–3332.
- Tozer, D.C., 1972. The present thermal state of the terrestrial planets. *Phys. Earth Planet. Inter.* 6, 182–197.
- van den Berg, A.P., van Keken, P.E., Yuen, D.A., 1993. The effects of a composite non-Newtonian and Newtonian rheology in mantle convection. *Geophys. J. Int.* 115, 62–78.
- van den Berg, A.P., Yuen, D.A., Steinbach, V., 2001. The effects of variable thermal conductivity on mantle heat-transfer. *Geophys. Res. Lett.* 28 (5), 875–878.
- van den Berg, A.P., Yuen, D.A., Allwardt, J.R., 2002. Nonlinear effects from variable thermal conductivity and mantle internal heating: implications for massive melting and secular cooling of the mantle. *Phys. Earth Planet. Inter.* 129, 359–375.
- van den Berg, A.P., Yuen, D.A., 2002. Delayed cooling of the Earth's mantle due to variable thermal conductivity and the formation of a low conductivity zone. *Earth Planet. Sci. Lett.* 199, 403–413.
- van der Hilst, R.D., Karason, H., 1999. Compositional heterogeneity in the bottom 1000 kilometers of Earth's mantle: toward a hybrid convection model. *Science* 283, 1885–1888.
- Zhang, S., Yuen, D.A., 1996. Various influences on plumes and dynamics in time-dependent, compressible, mantle convection in 3-D spherical shell. *Phys. Earth Planet. Inter.* 94, 241–267.